Meteorol. Atmos. Phys. 76, 119–141 (2001)

Meteorology and Atmospheric Physics

Geophysical Institute, University of Alaska Fairbanks, USA

On the uncertainty in mesoscale modeling caused by surface parameters

N. Mölders

With 11 Figures

Received September 9, 1999
Revised March 16, 2000

Summary

The uncertainty of plant- and soil parameters (albedo, evaporative conductivity, roughness-length, soil volumetric heat capacity, field capacity, capillarity, emissivity), soil-type, subgrid-scale heterogeneity and inhomogeneity on mesoscale model results (e.g., fluxes, variables of state, cloud- and precipitation-formation) is explored. Simulations are performed wherein one parameter at a time is changed for all grid cells of the domain within its natural range of variability. The land-surface scheme employs the frequently operated force-restore-method and a one-dimensional heat-diffusion equation. Transpiration is considered by the often applied "big-leaf/big-stoma"-approach.

Except for wind, cloud- and precipitating-particles the uncertainty in the simulated quantities due to soil- or plant-parameters is lower at night and in the early afternoon than at the other time of the day. Therefore, evaluation of meteorological models should be performed at those times when the sensitivity to the choice of plant- and soil-parameters is at a minimum. According to the calculated probability density functions and similarity coefficients, the partitioning of excess water vapor between cloud water and ice can be significantly affected by the choice of field capacity, capillarity, volumetric heat capacity, thermal diffusivity and the emissivity of the earth's surface. Considering these findings domain-specific and actual parameters should be preferred.

1. Introduction

Land-surface characteristics are important boundary conditions for mesoscale meteorological models to describe the exchanges of water, energy, and matter (e.g., carbon dioxide, isoprene, terpene, etc.). In numerical models, the complicated physical mechanisms of biosphere and geosphere and their interaction with the atmosphere must be parameterized. In these parameterizations, plant- and soil-physical characteristics must be simplified by few parameters. Thus, land-surface parameterization schemes usually apply prescribed values of soil- or plant-parameters either in some kind of "big-leaf/big-stoma"-approaches (e.g., Deardorff, 1978; Claussen, 1988; Groß, 1988; Schlünzen, 1994; Kramm et al., 1994; 1996; Chen and Dudhia, 2000; Mölders et al., 1999) or statistical-dynamical approaches based on the probability density functions of these parameters (e.g., Avissar, 1991; 1992). Doing so, pregiven parameter sets are assigned to each soil- and vegetation-type (e.g., Wilson et al., 1987; Dorman and Sellers, 1989; Table 1).

Ideally, the plant- and soil-characteristics should be mapped as continuous distributions to capture the gradients and mixtures in soil and vegetation within an area of interest (e.g., a grid-cell). However, to assign soil-physical parameters and/or a land-use-type to an area is not unambiguous (e.g., de Fries et al., 1995; Mölders et al. 1997a). Surface properties vary not only in space, but also in time. Herein, they may be influenced by previous weather conditions. Globally, vegetation characteristics vary by seasonality, growth, leaf type, water availability, elevation, terrain

slope, type and intensity of disturbance (e.g., fire history, cultivation, insects, drought, etc.). Soil hydraulic conductivity and albedo depend on soil moisture and thus on preceding precipitation. Nevertheless, if appropriately chosen, the combination of the surface parameters allows to reproduce the typical behavior associated with the various land-use types (Mölders, 1998).

Examining the impact of different data sets on the predicted variables of state, water and energy fluxes Mölders et al. (1997a) found that the distributions of daily averages of temperature and humidity will change less than 0.2 °C (1%) and 0.2 g/kg (1.5%) if the coverage of the various land-use and soil types differs only by about 5% between the data sets. Some locations, however, reveal appreciable differences in the daily averages of soil moisture ($0.19\,m^3\,m^{-3}$, 29%), surface temperature (2.3 °C, 12%), sensible ($30\,Wm^{-2}$, 29%) and latent heat fluxes ($32\,Wm^{-2}$, 34%).

Other recent studies demonstrated the influence of spatial variations of transpiring vegetation on the structure of the atmospheric boundary layer (ABL; e.g., Avissar and Pielke, 1989; Seth et al., 1994; Mölders and Raabe, 1996; Giorgi and Avissar, 1997). Doing so, various analyzing methods were applied. Zeng and Pielke (1995), for instance, used the scores typically used in meteorological evaluation studies to explore the influence of altered surface shape on moisture and heat fluxes. Analyzing the variability of surface fluxes by a Fourier amplitude sensitivity test Collins and Avissar (1994) examined the relative contribution of individual input parameters to the variance of energy fluxes. They found that most of the variability of surface heat fluxes may be described by the distribution of relative stomatal conductance and surface roughness.

For soil-types, it is even harder to get suitable (three-dimensional) data sets of soil parameters than for land-use. Thus, usually average parameters of the uppermost soil layer are applied for the entire soil depth. Results of off-line land-surface modeling (i.e., the feedback processes between the atmosphere and surface are not considered) with different soil hydraulic models, which were applied with and without making consistent soil hydraulic parameters, however, show that the uncertainties in soil hydraulic parameters overwhelm those in the theory of soil hydraulic models (Shao and Irannjad, 1999).

Land surface schemes are the only physical boundary condition in mesoscale atmospheric modeling. Previous studies mainly focused on the impact of soil- and plant-parameters on near-surface energy- and water fluxes in semi-arid areas (e.g., Avissar and Pielke, 1989). Moreover, most of these studies were offline or only two-dimensional. Thus, it is an urgent need to investigate the impact of these parameters also for humid mid-latitude conditions, where, for instance, water vapor deficit is often low and clouds exist frequently. Since the temperature and moisture states in the system earth-atmosphere evolve by fluxes that themselves depend on those states, the choice of these parameters may be much more far-reaching. It has to be expected that the choice of plant- and soil-parameters may affect the local recycling of precipitation, i.e. the cloud- and precipitation formation within an area. It is the aim of this study to exemplarily examine this uncertainty in simulation results. Herein, the influence of these parameters on the statistical amount of cloud- and precipitating-particles as well as the temporal development of uncertainty will be focused on. Furthermore, the results will be elucidated in the context of the results from previous studies.

2. Model description

The non-hydrostatic meteorological model GESIMA (Geesthacht's Simulation Model of the Atmosphere; Kapitza and Eppel, 1992; Eppel et al., 1995) is used in this study. This model and its modules were validated for a wide range of phenomena (e.g., Claussen, 1988; Kapitza and Eppel, 1992; Levkov et al., 1992; Eppel et al., 1995; Devantier and Raabe, 1996; Hinneburg and Tetzlaff, 1996; Mölders, 1998; Fritsch, 1999). Moreover, it was shown that GESIMA is able to simulate the typical behavior associated with the various land-use types (Mölders, 1998).

2.1 Dynamics

The dynamic part of GESIMA is based on the equation of continuity used in the anelastic approximated form (i.e., $\partial\bar{\rho}/\partial t = 0$) to suppress sound waves, the conservation equations for

momentum, energy, and various atmospheric constituents like dry air, water vapor, liquid water, and ice as well as the equation of state (Kapitza and Eppel, 1992; Eppel et al., 1995). In recognition of the turbulent state in the troposphere, all equations are averaged according to Reynolds and have been, in a further step, Boussinesq-approximated (see Kapitza and Eppel, 1992).

2.2 Clouds and radiation

Cloud processes are taken into account by a parameterization of bulk-microphysics. This parameterization considers the condensation and deposition of water vapor, the rainwater formation by autoconversion, coalescence and melting of ice and graupel, the riming of ice and graupel by cloud water, the homogeneous freezing of cloud water and rainwater, the evaporation of cloud water and rainwater, the sublimation of ice and graupel, the sedimentation of rainwater, ice, and graupel (Mölders et al., 1997b). A simplified two-stream method serves to calculate the radiative transfer (Eppel et al., 1995).

2.3 Soil and vegetation

Soil-wetness is determined by a force-restore-method (Deardorff, 1978). At the surface, a bulk-parameterization is applied to calculate the fluxes of sensible and latent heat. To determine the transpiration by plants, a Jarvis-type (Jarvis, 1976) approach is considered for the bulk-stomatal conductance (Eppel et al., 1995; Mölders, 1998). Sensitivity of bulk-stomatal resistance against evapotranspiration to photosynthetic active radiation, leaf temperature, water vapor deficit between leaf and ambient air as well as soil moisture deficit (Jarvis, 1976; Hicks et al., 1987) is taken into account by correction functions that range between 0 and 1. Like in many other land surface schemes (e.g., Chen and Dudhia, 2000) a single linearized surface energy balance equation representing the combined ground/vegetation surface is solved to determine skin temperature. The soil heat-fluxes and soil temperatures are calculated by a one-dimensional heat-diffusion equation (cf. Eppel et al., 1995).

This land surface scheme has been validated for a wide range of cases (e.g., Claussen, 1988; Mölders, 1998; Fritsch, 1999). Similar schemes are used, for instance, in METRAS (e.g., Schlünzen, 1994) and FITNAH (e.g., Groß, 1988).

The surface stress and near-surface fluxes of heat and water vapor are expressed in terms of dimensionless drag coefficients and transfer coefficients of heat and moisture applying a parametric model (Kramm et al., 1995) which is based on Monin-Obukhov similarity theory.

2.4 Turbulence

For the region above the surface-layer the turbulent flux of momentum is calculated by a one-and-a-half-order closure scheme. Here, the elements of the eddy-diffusivity tensor are expressed by the vertical eddy diffusivity $K_{M,V}$, and horizontal diffusivity, $K_{M,H}$, where the latter is also related to $K_{M,V}$ by the simple linear relationship $K_{M,H} = 2.3\,K_{M,V}$. Furthermore, $K_{M,V}$ is expressed by the turbulent kinetic energy (TKE) and mixing length, applying the Kolmogorov-Prandtl relation. Here, the mixing length is parameterized by Blackadar's (1962) approach, slightly modified by Mellor and Yamada (1974). The turbulent fluxes of sensible heat and water vapor for that region are expressed as functions of $K_{M,V}$ and the turbulent Prandtl-number, $Pr_t = K_{M,V}/K_{H,V}$, and turbulent Schmidt-number, $Sc_t = K_{M,V}/K_{E,V}$, respectively. These characteristic numbers are considered to be functions of the thermal stratification. They are derived from the local stability functions of Businger et al. (1971) and the assumption that $Sc_t = Pr_t$. To determine the TKE, an additional budget equation for that quantity is solved where the energy production, due to horizontal shear, is neglected (see Kapitza and Eppel, 1992).

2.5 Subgrid-scale heterogeneity and inhomogeneity

Subgrid-scale heterogeneity is considered by an explicit subgrid-scheme (Seth et al., 1994; Mölders et al., 1996), where the vegetation- and soil-types are realized by different dynamic, hydrologic, and energetic quantities (Table 1). This scheme determines the water- and energy fluxes, soil-wetness factors, soil and surface temperatures on a finer grid resolution than that used for the whole model domain. The subgrid-cells are considered to be homogeneously covered by their

Table 1. Parameters (from Eppel et al., 1995 and references therein) as used for the different land-use types in the soil-vegetation model. The letters $k_s, \rho_s c_s, \varepsilon, \alpha, z_0, w_k, \alpha_c$, and g_1 represent thermal diffusivity of soil, volumetric heat capacity, emissivity, albedo, roughness length, field capacity, capillarity, and maximum evaporative conductivity, respectively. The quantities indicated by * are calculated by the model

Land-use type	α	ε	z_o	k_s	$\rho_S c_S$	w_k	α_c	g_1
				10^{-6}	10^6		10^{-3}	
			m	m^2/s	$J/(m^3K)$	m	$kg/(m^3s)$	m/s
Sea deeper than 10 m	*	0.95	*	0.14	4.2	1.0	1000	–
Sea less than 10 m deep	*	0.95	*	0.14	4.2	1.0	1000	–
Waters	*	0.94	*	0.15	4.2	1.0	1000	–
Sand	0.3	0.90	0.0004	0.84	2.1	0.002	0.9	–
Grassland	0.25	0.95	0.02	0.56	2.1	0.010	8.0	0.04
Agriculture	0.18	0.95	0.04	0.74	2.9	0.005	3.0	0.04
Heath	0.15	0.95	0.35	0.70	2.5	0.003	1.0	0.024
Deciduous forest	0.20	0.97	0.8	0.70	2.5	0.010	8.0	0.023
Mixed forest	0.175	0.975	0.9	0.70	2.5	0.010	8.0	0.023
Coniferous forest	0.15	0.98	1.0	0.70	2.5	0.010	8.0	0.023
Village/suburbs	0.20	0.90	0.8	1.0	2.0	0.003	1.0	–
City	0.15	0.95	1.0	1.0	2.0	0.002	0.9	–

individual vegetation over horizontally homogeneous soil-types. A fundamental assumption of this strategy is that the subgrid-scale near-surface meteorological forcing, which is experienced by the surface, is important in determining the net exchange of heat, moisture, and momentum at the earth-atmosphere interface, i.e. the horizontal fluxes between different subgrid-cells within a cell are small in comparison to the corresponding vertical transfer processes. Thus, no direct horizontal interaction between different vegetation-types exists. The use of mean wind vector for the entire grid-cell means that no effects on the magnitude and direction of wind as well as subgrid-scale dynamic effects related to surface heterogeneity (e.g., directed flows caused by topography) are considered. Such advective effects are accompanied by occasionally observed internal boundary layers (Raabe, 1983; Garratt, 1992; Hupfer and Raabe, 1994). Of course, such effects may differently influence the fluxes calculated for different subgrid-cells and demand further research.

In the case that precipitation is also heterogenized, not only subgrid-scale heterogeneity, but also subgrid-scale inhomogeneity can be considered. When heterogenizing precipitation, subgrid-cells of equal land-use may have different soil moisture, and, thus, different surface fluxes and soil temperatures. This means that, within a grid-cell, a seemingly equal area (of same land-use) is inhomogeneous with respect to its soil physical state and near-surface fluxes.

2.6 Boundary conditions and numerical treatment

At the top of the model, a rigid lid, together with a sponge layer to absorb vertically propagating gravity waves, is used. At the lateral boundaries, Orlanski's (1976) radiation-boundary conditions are applied for the normal component of momentum. A zero-gradient method is applied for all other variables. As a final step the resulting normal mass fluxes are adjusted to comply with mass continuity.

The prognostic equations are solved with a predictor/corrector scheme. Advection of momentum and sensible heat is treated with a modified MacCormack-scheme as cited by Anderson et al. (1984); whereas advection of the aforementioned trace constituents is dealt with the Smolarkiewicz-scheme (Smolarkiewicz, 1984). Horizontal diffusion is calculated explicitly, while any vertical diffusion is computed implicitly.

2.7 Model domain

The domain under investigation encompasses the troposphere over the mouth of river Elbe and parts of the western Baltic Sea from the surface to a height of 10.5 km with a horizontal extension of

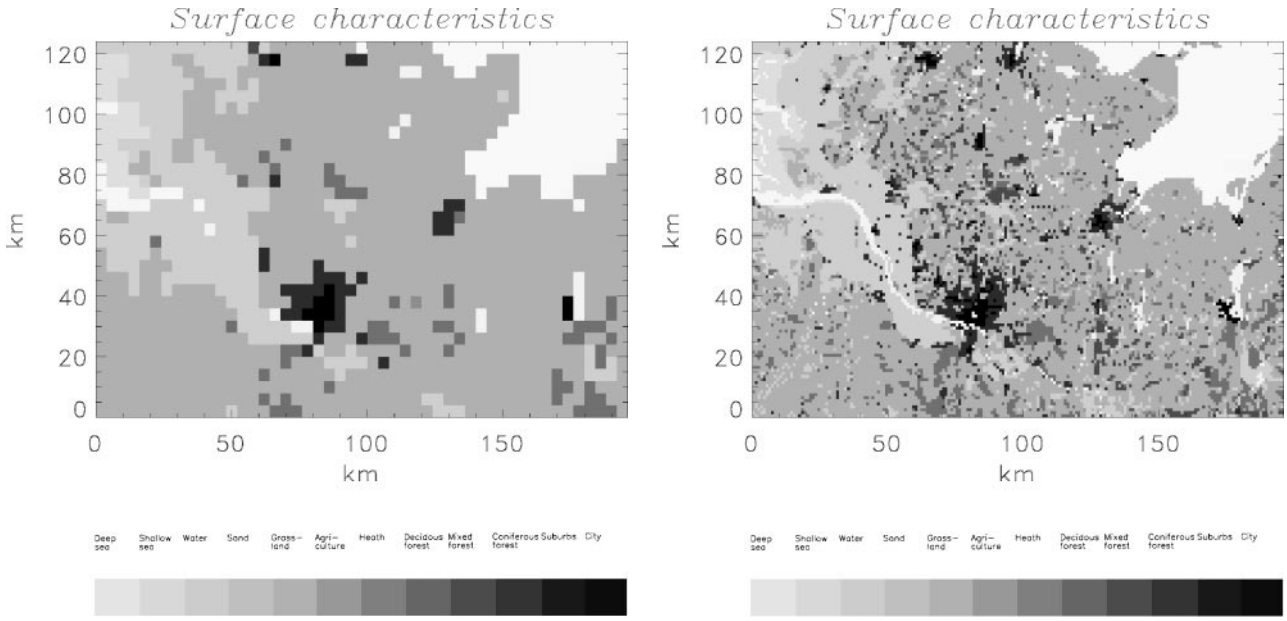

Fig. 1. Schematic view of plant- and soil-parameter distributions (Table 1) as used in the study (left) without and (right) with consideration of subgrid-scale heterogeneity (modified after Mölders and Raabe (1996))

(the inner grid of) 124 km in north-south and 196 km in west-east direction (Fig. 1). This inner domain is surrounded by an outer grid (five grid points). These outer boundary values are not considered for the evaluation of the simulation results. The region is characterized by relatively flat topography, strongly eroded heterogeneous soils, shallow water tables, water meadows, bogs, small lakes, and settlements.

The vertical resolution of the model varies from 20 m close to the ground to 1 km at the top of the model. Eight levels are located below 2 km and 8 above that height. The horizontal resolution is $4 \times 4\,km^2$ for the atmospheric grid (Fig. 1 left) and $1 \times 1\,km^2$ for the subgrid (Fig. 1 right). Since the subgrid-mesh amounts to one kilometer, the reference height is chosen as 10 m to meet those fetch conditions (ratio of vertical to horizontal of 1:100; e.g., Raabe, 1983; Garratt, 1992) that were realized during the field experiments from where the empirical quantities of the Monin-Obukov similarity theory originate.

2.8 Initialization

All three-dimensional-simulations are initialized with the same profiles of wind, moisture, air and soil temperature obtained from a one-dimen-

Table 2. Initial conditions

Geostrophic wind and direction at a height of 10.5 km				$5\,m\,s^{-1}$ from SW				
Soil wetness factor				0.17				
Soil temperature in 1 m depth				280 K				
Sea surface temperature for sea deeper than 10 m				277 K				
Sea surface temperature for sea less than 10 m deep				279 K				
Water surface temperature				283 K				
Julian day				116				
Height (m)	10	40	155	350	600	875	1250	1750
Temperature (K)	276.9	278.3	278.7	276.8	274.2	271.5	267.7	264.4
Humidity ($g\,kg^{-1}$)	3.147	3.147	3.125	3.118	3.114	3.107	3.080	1.250
Height (m)	2500	3500	4500	5500	6500	7500	8750	10250
Temperature (K)	262.2	254.9	248.4	238.2	232.7	222.7	228.5	227.1
Humidity ($g\,kg^{-1}$)	1.405	1.487	0.469	0.421	0.126	0.107	0.157	0.089

sional-simulation (Table 2) that adjusts the vertical profiles of temperature and wind speed to homogeneous terrain. These profiles are orientated at typical synoptic situations in spring when an anticyclone over northeastern Europe, a weakening, slowly eastwards moving cyclone near Iceland, and an intensifying, northwards moving low over the Alps govern the weather in the domain of interest.

3. Design of the study

In the system earth-atmosphere, the fluxes, temperature and moisture states are closely related to the surface characteristics that are not exactly known. To investigate the uncertainty caused by the choice of surface parameters, a set of simulations is performed with GESIMA using its original (Table 1) and altered parameters (Table 3). In each simulation, one parameter at a time (e.g., albedo) is changed for all land-use- and soil-types according to Table 3, while all other parameters are taken from Table 1. Out of the abundance of possible variations of these parameters, one change is performed for each parameter. In a further set of simulations, subgrid-scale heterogeneity is considered alternatively with and without subgrid-scale inhomogeneity. In addition, a simulation is carried out assuming that, in the entire domain, the soil is sandy loam.

Since there exist no observational data at the resolution of the model the results obtained by the simulation with the parameters of Table 1 are arbitrarily taken as "grand truth". Thus, to elaborate the uncertainty resulting from soil- and plant-parameters, the results of all sensitivity studies are compared with these reference data.

Furthermore, out of the variety of statistical methods, probability density functions and similarity coefficients are chosen to evaluate the results. Probability density functions namely allow to elucidate the shift in the statistical behavior of the fluxes, variables of state as well as cloud- and precipitating-particles. The similarity coefficients give a measure how strongly the results differ. They identify those surface characteristics to which the results are the less sensitive, i.e. which surface parameters yield similar results with respect to the surface parameters taken in the reference simulation. Furthermore, they allow to detect the time variance of uncertainty. The identification of insensitive parameters may provide hints how land surface schemes can be simplified.

Looking at the daytime surface moist static energy flux

$$h = H + LE = (1 - \alpha)R_{S\downarrow} - R_{L\uparrow} - G, \qquad (1)$$

where H and LE are the sensible and latent surface heat fluxes, and $\alpha, R_{S\downarrow}, R_{L\uparrow}$ and G represent the surface albedo, downward shortwave radiation, upward net longwave radiation, and soil heat flux, respectively. As long as the right hand side is not altered by the parameter modifications, moist static energy does not change. However, the partitioning between the sensible and latent heat fluxes may be affected by heterogeneity and parameter choice and, hence, the ratio between these fluxes (Bowen-ratio) may change (e.g.,

Table 3. As Table 1, but parameters as used for the sensitivity studies. Note that only one parameter at a time, for instance albedo, is changed for all land-use types. The other parameters are taken from Table 1. Note that for the water surfaces pregiven parameters were not changed

Land-use type	α	ε	z_o	k_s	$\rho_S c_S$	w_k	α_c	g_1
				10^{-6}	10^6		10^{-3}	
			m	m^2/s	$J/(m^3K)$	m	$kg/(m^3s)$	m/s
Sand	0.27	1	0.0008	0.924	2.31	0.004	1.8	–
Grassland	0.225	1	0.04	0.616	2.31	0.020	16.0	0.08
Agriculture	0.162	1	0.08	0.814	3.19	0.010	6.0	0.08
Heath	0.135	1	0.7	0.77	2.75	0.006	2.0	0.048
Deciduous forest	0.18	1	1.6	0.77	2.75	0.020	16.0	0.046
Mixed forest	0.1575	1	1.8	0.77	2.75	0.020	16.0	0.046
Coniferous forest	0.135	1	2.0	0.77	2.75	0.020	16.0	0.046
Village/suburbs	0.18	1	1.6	1.1	2.2	0.006	2.0	–
City	0.135	1	2.0	1.1	2.2	0.004	1.8	–

Friedrich, 1999; Friedrich et al., 2000). Reduced albedo would increase the moist static energy. An increase in Bowen-ratio means a decrease in moist static energy which potentially reduces convection. For the these reason, here, the Bowen-ratio is also used to evaluate the simulation results.

3.1 Probability density functions

Following Entekhabi and Brubaker (1995) and Hantel and Acs (1998), the statistical behavior of the effects of different surface parameters is evaluated by frequency distributions of simulated water- and energy fluxes, state quantities as well as cloud- and precipitating-particles. Probability density functions are determined for the entire integration time using the hourly data provided for the inner grid by the different simulations. The probability density function of a quantity is given by (e.g., Olberg and Rakóczi, 1984)

$$pdf(\chi) = p(\chi \leq X \leq \chi + \Delta X)/\Delta X, \tag{2}$$

where p is the frequency in the interval $(\chi, \chi + \Delta X)$. The probability density functions are based on $49\times31\times24$ values for each quantity regarded at the surface (e.g., surface temperature, soil wetness, surface fluxes) or at reference height (e.g., wind, air temperature, humidity). They are based on $49\times31\times16\times24$ values for quantities regarded all over the entire inner domain (e.g., cloud water, rainwater, ice).

3.2 Similarity coefficients

Ogunjemiyo et al. (1997) modified a given procedure by Jackson et al. (1989) for comparing data fields containing different parameters or for comparing data fields of same parameters that are recorded at different times. Friedrich (1999) modified this method for comparing results obtained by simulations assuming different land-use distributions. In the present study, this procedure is adapted for comparing the results obtained by the sensitivity simulations to those of the reference simulation. The simulated quantities (e.g., variables of state, fluxes, cloud- and precipitating-particles), X_{ij}, at the grid-point i,j on the distribution field are transformed into a set of values Z_{ij}, by subtracting the domain-averaged value $\bar{X}$ and normalizing the difference by the standard deviation of the differences S (see Ogunjemiyo et al., 1997)

$$Z_{ij} = \frac{X_{ij} - \bar{X}}{S}. \tag{3}$$

The similarity between two transformed distributions is now established on the basis of similarity in the sign of Z_{ij}-pairs (Ogunjemiyo et al., 1997) as

$$C_s = \frac{m + p}{m + n + p}, \tag{4}$$

where C_s is the similarity coefficient, m, n, and p are the numbers of Z_{ij}-pairs with mixed, negative, and positive signs. The similarity coefficient ranges from zero (no similarity) to 1 (absolute agreement).

4. Results and discussion

Generally, the absolute differences in all quantities are greater during daytime than nighttime because of the strong interrelation between the atmospheric water cycle and the energy budget. However, in the upper troposphere, predicted temperature, humidity, and cloud distributions are hardly affected. In cloudy regions, somewhat greater differences occur resulting from differences in phase transition processes, vertical motions, turbulence or radiative cooling. Compared with the mid and upper troposphere, the uncertainties in the predicted variables of state caused by the choice of plant- and soil-parameters are greater in the ABL. Here, the differences in humidity and air temperature increase when approaching the earth's surface. Generally, below clouds, differences in evaporation of rainwater or sublimation of ice more strongly affect the distribution of specific humidity than the differences in evapotranspiration. Note that the quantitative effects of altered plant- and soil parameters are independent of the cloud-parameterization schemes applied (Mölders, 1999).

As compared to the reference simulation, simulated air- and ground-temperatures, humidity, soil moisture, and cloud distributions will differ more strongly than for the other parameter changes if (1) capillarity is doubled, (2) surface emissivity is set equal to 1, (3) volumetric heat capacity or (4) thermal diffusivity are enhanced by 10%, or subgrid-scale heterogeneity (5) with and

(6) without subgrid-scale inhomogeneity are taken into account. The variables of state, fluxes, cloud- and precipitating-particles predicted by the simulations with (1) a homogeneously sandy loam, (2) a 10% reduced albedo, (3) a doubled evaporative conductivity or (4) roughness length only slightly differ from those of the reference simulation. The horizontal wind field will be altered significantly at some locations if thermal diffusivity or alternatively volumetric heat capacity are increased by 10%. For brevity, only the impact on predicted variables of state, cloud- and precipitating-particles, or fluxes is discussed in detail for those parameters that cause appreciable uncertainties.

Generally, primary differences result from the changed plant- or soil-parameters. The mass-weighted saturation mixing ratio (Mölders et al., 1997b) leads to secondary differences from the specific saturation mixing ratios. As in nature, namely in a warmer atmosphere, less cloud water and ice are formed and less rainwater is built than in a cooler one. This means that if the choice of plant- or soil-parameters modifies air temperatures, the partitioning between the cold and warm path of precipitation formation processes will be altered, too. This fact is manifested by a shift in the probability density distribution. In addition, a warmer and drier ABL leads to a retarded onset of cloud-formation and higher levels of cloud bases.

On average, net radiation and soil heat fluxes are appreciably affected when cloudiness is modified due to the other choice of soil or plant parameters. The changed distribution of net radiation again modifies the fluxes of sensible and latent heat.

4.1 Radiative properties

Various land surface schemes apply the "big-leaf/big-stoma"-approach. Herein, either a shielding factor of 1 (totally covered by plants) or 0 (bare soil; e.g., Schlünzen, 1994), or fractions of vegetation cover (e.g., Deardorff, 1978; Kramm et al., 1996) are assumed. In the latter case, often a single skin temperature for the foliage and bare soil is determined (e.g., Chen and Dudhia, 2000) and the emissivity or albedo of the soil and the foilage are not distinguished. Therefore, the uncertainty of albedo and emissivity is addressed.

4.1.1 Albedo

Albedo, among others, depends on latitude, diurnal course, season, cloudiness, terrain-slope, soil moisture, soil- and/or vegetation-type (e.g., Idso et al., 1975; Baumgartner et al., 1977; Sellers et al., 1986; Pielke, 1984) as well as on wind speed (e.g., Betts and Ball, 1997). Over areas of several square kilometers, the spatial variability of albedo may even vary more than 10% – snow-covered areas excepted (e.g., Pielke et al., 1993). The albedo of various soils ranges from 0.05 to 0.35 (e.g., Pielke, 1984). The albedo of grass varies from 0.16 to 0.3 (e.g., Pielke, 1984) where the individual variability within a given community may be even smaller. Betts and Ball (1997), for instance, determined the time-averaged mean albedo of grass from long-term observations at the same location as 0.194 with a standard-deviation of ± 0.021. For aspen, pines and spruce the standard-deviation also amounts about 10% of the mean value (see, e.g., Betts and Ball, 1997).

Surface-albedo is reduced by 10% (cf. Tables 1, 3) to examine the uncertainty caused by the choice of this parameter. This reduction leads to an increase of the fluxes of sensible and latent heat as well as vertical motions. It results in a higher probability of greater values of specific humidity, cloud-water, rain-water, and ice with increasing simulation time. Thus, precipitation is intensified locally up to more than 4%. Consequently, soil moisture increases. These findings substantially agree with Charney (1975).

In addition, in the present study, it was found that reducing the albedo leads to a larger extension of the areas receiving precipitation than in the reference simulation. Consequently, soil temperature distribution is smoothed and extreme values of soil temperature occur less frequently.

4.1.2 Emissivity

Emissivity of vegetation, water, and soils varies with space and time. Although the earth's surface does not radiate like a black body, it is often dealt like a black body in mesoscale models (cf. Pielke, 1984). Here, a sensitivity study is performed assuming a surface emissivity of 1 for all surfaces.

Net radiation and soil heat fluxes grow appreciably due to the increased emissivity. Here among other, the altered cloudiness (see also

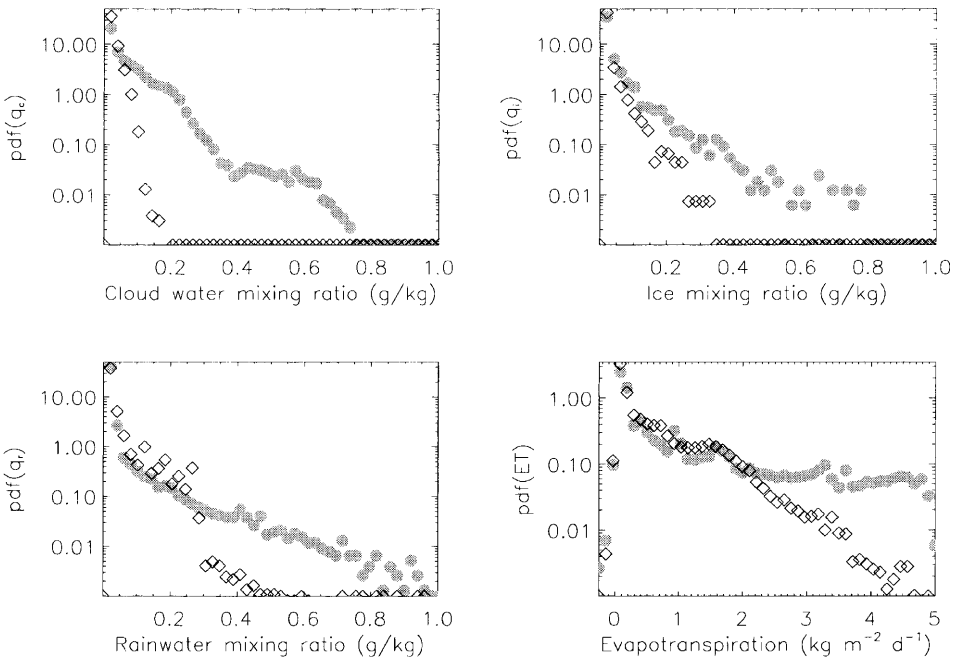

Fig. 2. Comparison of probability density functions of cloud water, q_c, ice, q_i, rainwater, q_r, in g/kg and evapotranspiration, ET, in kg m^{-2} d^{-1} (upper left to lower right) as determined for the reference simulation (grey circles) and the simulation with a surface emissivity equal to 1 (diamonds). Note that y-axis is logarithmic and that for evapotranspiration scaling of the x-axis differs from that of the water substances

Fig. 2) plays a role. Due to the modified insolation the partitioning of incoming solar energy shifts towards lower evapotranspiration rates for a surface emissivity of 1 (Fig. 2). Herein, at some locations, the fluxes of sensible and latent heat decrease up to 50 Wm^{-2}. Nevertheless, on average, lower Bowen-ratios are achieved for a surface emissivity of 1 than in the reference case (not shown).

On average, a surface emissivity of 1 yields to a cooler (locally more than 1 K) and drier (locally more than 0.6 g/kg) ABL than the emissivities taken in the reference simulation. Moreover, ground temperatures decrease up to 5 K. The frequency of high mixing ratios of cloud- and precipitating-particles is reduced in favor of a higher frequency of lower values (e.g., Fig. 2). Consequently, maximum precipitation decreases. The cloud- and precipitation patterns alter appreciably, too.

Note that, in stationary one-dimensional studies (e.g., Friedrich, 1999), a surface emissivity of 1 causes smaller differences than in three-dimensional studies. Obviously, in the latter, the feedback processes with altered cloudiness (e.g., Fig. 2) and the modified dynamical behavior of the atmosphere, especially in the ABL, play a role that should not be underestimated. A possible reason may be the grid-scale generated fluxes because the horizontal scale interaction in the free atmosphere is physically different from that at the surface (e.g., Hantel and Acs, 1998).

4.2 Aerodynamical properties

Many modern mesoscale models apply a one-and-a-half order closure model to describe momentum transfer properties. The roughness length influences the magnitude of the aerodynamic resistance and the near-surface drag force. Here, roughness length is not intended as catch all surface parameters to specify total surface generated drag, i.e. topographically induced effects are not addressed.

4.2.1 Roughness length

Roughness length ranges from 10^{-5} m over smooth ice to 10 m over high buildings (e.g., Oke, 1978). Over some surfaces, for instance, long grass or water, the roughness length may be expressed as a function of friction velocity (e.g., Pielke, 1984). Usually, roughness length is assumed to be equal

to 10% of canopy height. Such an approach, however, ignores the density of stand, form of object and spatial distribution of roughness elements (e.g., Oke, 1978). As shown by Kramm (1995), the relationship between roughness length and canopy height, z_0/h, decreases with increasing height of stand, h. Since canopy height varies in space and time, the roughness length of a given vegetation-type may alter more than one order of magnitude (e.g., Pielke, 1984).

Previous studies found roughness length to have a great impact on surface fluxes (e.g., Collins and Avissar, 1994). Here, however, the effect of roughness length is less strong than that reported by the other authors probably because they performed an off-line study.

In addition, here, the influence of doubling roughness length (see Table 3) on simulated variables of state as well as cloud- and precipitating-particles is elucidated. The increased roughness length modifies mixing and thus, the mechanical state of turbulence. Low-level moisture convergence, ground temperatures, Bowen-ratios, the mixing ratios of precipitating particles, and strong precipitation only slightly increase, while the mixing ratios of cloud water and light precipitation decrease slightly (not shown). However, it seems worth mentioning that the positions of the cloud- and precipitation fields shift (about 4 km) upstream.

4.3 Soil physical properties

In nature, soil temperature and soil moisture are coupled. A temperature gradient can cause a change in soil volumetric water content (Ludwig-Soret-effect) and a moisture gradient may alter soil temperature (Dufor-effect). Since on short time scales thermal conductivity (= thermal diffusivity times heat capacity) and volumetric heat capacity of the substrate influence each other only slightly, these effects are usually neglected in short-term predictions. Thus, decoupled equations to describe the energy- and water-transport within the soil are commonly applied (e.g., Deardorff, 1978; McCumber and Pielke, 1981; Groß, 1988; Schlünzen, 1994; Jacobson and Heise, 1982; Eppel et al., 1995; Chen and Dudhia, 2000). The effects of the parameters required in the heat diffusion equation on simulated results are evaluated in subsection 4.3.1.

Soil wetness is frequently calculated by a two-layered force-restore-method (e.g., Deadorff, 1978; Groß, 1988; Schlünzen, 1994; Jacobson and Heise, 1982). The impact of the parameters needed therein on the simulated results is given in subsection 4.3.2. Subsection 4.3.3 addresses the problem of insufficiently known soil type.

4.3.1 Thermal diffusivity and volumetric heat capacity

Heat capacity increases with increasing soil moisture for most of the soils (e.g., Oke, 1978). Figure 3 exemplarily illustrates for three soil-types the dependence of thermal diffusivity on relative volumetric water content. Thermal diffusivity is more than twice as high for a relative volumetric water content of 0.5 than of 1 (at saturation; Fig. 3).

Since, as will be explained later, soil moisture is usually much lower than saturation, thermal diffusivity and volumetric heat capacity are enhanced one at a time by 10% of their values in Table 1 (see Table 3) to elucidate the sensitivity of meteorological predictions to these parameters. Comparing the results of these studies with those of the reference simulation substantiates that the bimodal structure of the frequency distribution of the soil heat fluxes weakens and the distribution becomes smaller (e.g., Fig. 4; Note that the frequency distributions for the surface fluxes look quite similar for a 10% increased volumetric heat capacity therefore not shown.). The frequency of high sensible and latent heat fluxes decreases in

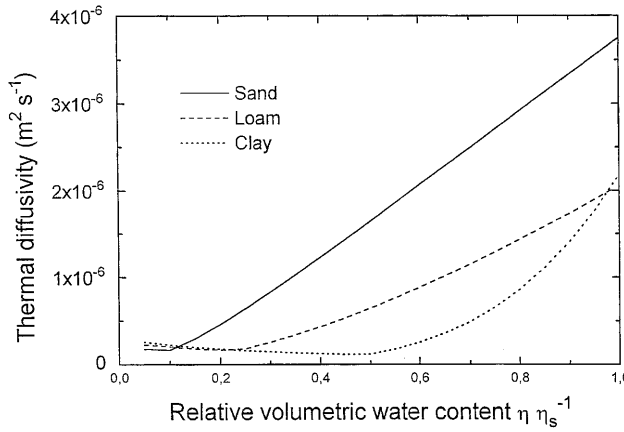

Fig. 3. Dependence of thermal diffusivity on relative volumetric water content (determined as the ratio of actual water content, η, to that at saturation, η_s)

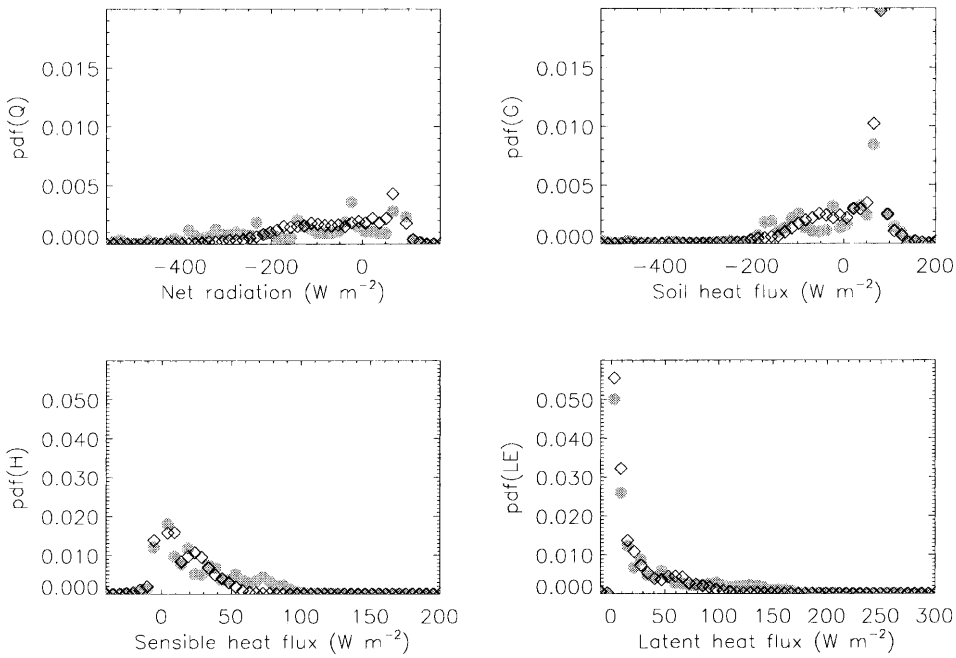

Fig. 4. Comparison of probability density functions of net radiation, Q, soil heat fluxes, G, sensible, H, and latent heat fluxes, LE, (upper left to lower right) all in Wm^{-2} as determined for the reference simulation (gray circles) and the simulation with a 10% increased thermal diffusivity (diamonds). Note that scaling of the x- and y-axis is different for the various quantities

favor to lower values (e.g., Fig. 4). Like for an emissivity of 1 the partitioning of incoming energy shifts towards lower Bowen-ratios (not shown).

On average, in the case of enhanced thermal diffusivities or volumetric heat capacities, the ABL and soils are cooler (locally more than 1 K and 5 K, respectively) than in the reference simulation. Specific humidity, cloud water, rainwater, and ice as well as maximum precipitation decrease for enhanced volumetric heat capacities or thermal diffusivities (not shown).

4.3.2 Soil hydraulic properties

Cuneca et al. (1996) investigated soil water parameterizations. They found that the variations exhibited in the surface fluxes are unexpectedly large. In off-line studies, soil hydraulic conductivity was pointed out to cause severe changes in surface fluxes (Gao et al., 1996). Since these parameterizations and the associated parameters are not required in the force-restore-method, here, the impact of its soil hydraulic properties on simulated fluxes, variables of states, cloud- and precipitating-particles is explored by alternatively doubling field capacity or capillarity (Tables 1, 3).

4.3.2.1 Field capacity

Field capacity depends, among others, on soil structure and -texture, grain size distribution, permeability, temperature, and air pressure. The field capacity of recultivated areas, for instance, varies more than 20%, on average (e.g., Wünsche, 1995).

Field capacity is usually defined as that value of water content remaining in the soil after downward gravity drainage has ceased (Bear, 1988). However, this definition is not a quantitative specification of what is meant by materially ceased. Therefore, this point is frequently discussed in the literature (e.g., Bear, 1988).

Consequently, there also exists a variety of different formulations of field capacity in up to date land surface schemes (e.g., Eppel et al., 1995; Cuneca et al., 1996; Chen and Dudhia, 2000). In land surface schemes of the force-restore type (e.g., Deardorff, 1978; Jacobson and Heise, 1982; Groß, 1988; Schlünzen, 1994) like investigated here, field capacity requires an integral value representative for the uppermost soil layer. Thus, this value depends on the thickness of this layer.

Evapotranspiration increases for great evapotranspiration rates, while it decreases for inter-

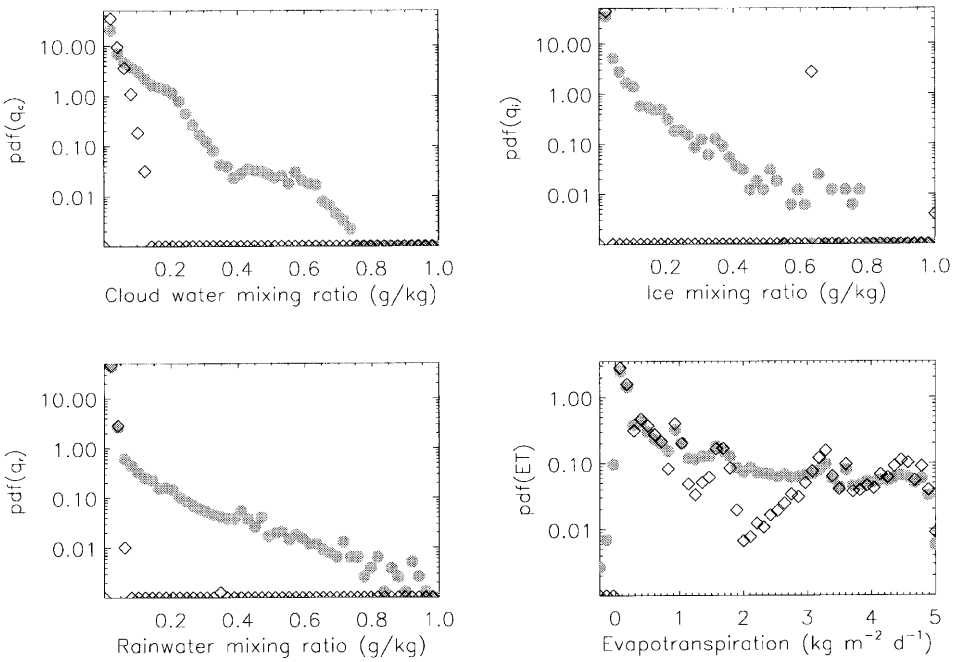

Fig. 5. Like Fig. 2, but for the reference simulation (gray circles) and the simulation with a doubled field capacity (diamonds)

mediate rates (Fig. 5). Changes are greater in areas of intermediate and high evapotranspiration, e.g., after precipitation or over the water meadows. This finding is not surprising. Owing to the atmospheric demands by evapotranspiration, in the model as well as in nature, soil wetness is usually below field capacity for most of the time and most locations.

Doubling field capacity, on average, yields a moister and warmer lower ABL as well as slightly higher surface temperatures than in the reference simulation (not shown), although there is a slight shift of the maximum and the minimum values towards lower values. Compared with the results of the reference simulation the mixing ratios of cloud water, rainwater, and ice, precipitation intensity as well as the extension of the precipitation fields slightly decrease when field capacity is doubled. In particular, high mixing ratios (>0.15 g/kg) that seldom occur in the reference simulation, do not occur at all (Fig. 5).

4.3.2.2 Capillarity

Below field capacity, soils contain capillary water, in form of continuous films around the soil particles that are held by surface tension. This water is available to plants (e.g., Bear, 1988). By capillary rise water may move from a near-surface water table or dammed water, or water may reach the root zone or the earth's surface if evapotranspiration removes so much water that an upwards directed hydraulic gradient develops. Thus, besides the soil physical and geological conditions, capillary rise depends on vegetation and atmospheric conditions (see also Baumgartner and Liebscher, 1990).

In this study, a simulation is performed assuming a double as high capillarity than in Table 1 (Table 3). On average, in the simulation with doubled capillarity, the probability density functions of net radiation and soil heat fluxes shift towards higher values (e.g., Fig. 6). Like for an emissivity equal to 1, increasing thermal diffusivity or volumetric heat capacity by 10%, the Bowen-ratios decrease as compared with the reference simulation.

Doubling capillarity yields to a decrease of soil temperatures, near-surface air temperatures, humidity, specific mixing ratios of cloud- and precipitation particles, precipitation as well as the fluxes of sensible and latent heat as compared to the reference simulation (e.g., Fig. 6). At some locations, soil temperatures, air temperatures, and specific humidity differ more than 2 K, 0.5 K, and up to 0.5 g/kg, respectively. Furthermore, the near-surface wind field changes appreciably due to the modified cloudiness (not shown).

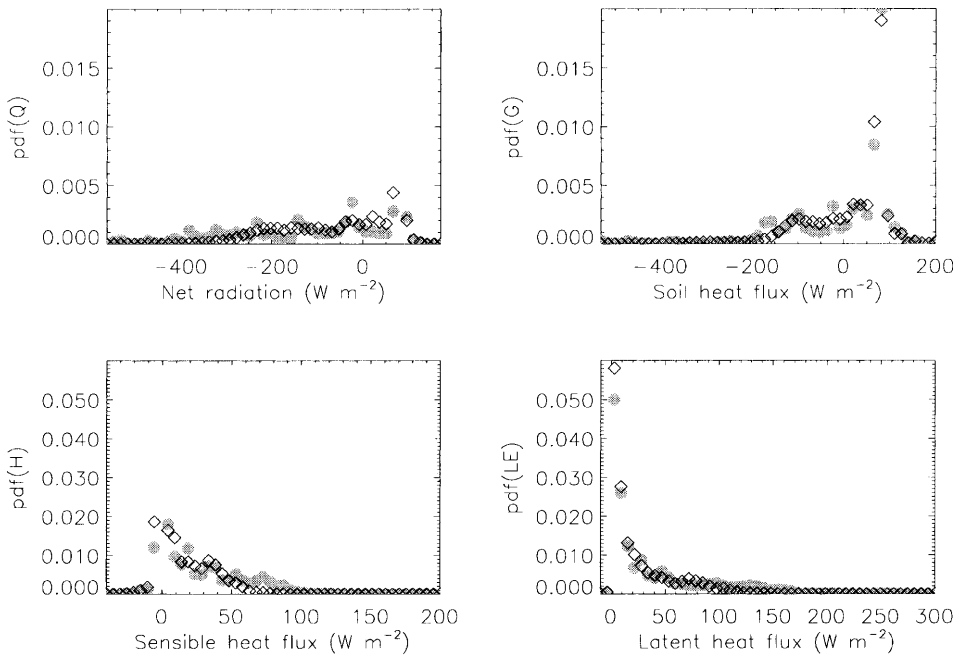

Fig. 6. Like Fig. 4, but for the reference simulation (gray circles) and the simulation with a doubled capillarity (diamonds)

4.3.3 Soil-type

According to the theory developed by Eagleson (1982), in which climate, soil, and vegetation evolve synergetically, in many atmospheric models, soil-type is related to land-use (e.g., Eppel et al., 1995). Cereals, for instance, grow better on heavier, more loamy soils compared with vines that grow better on sandy soil. Areas of same land-use with different soil-types may yield different evapotranspiration rates under the same meteorological conditions. These differences increase with decreasing soil wetness and with increasing differences in soil wetness of various soils (Keese, 1997; personal communication).

Thus, the uncertainty in predicted quantities and fluxes that is caused by an inaccurate choice of soil-type is examined. Herein, the entire model domain is covered by a sandy loam ($k_s = 0.73 \cdot 10^{-6}\,\mathrm{m^2/s}$, $c_s\rho_s = 2.1 \cdot 10^6\,\mathrm{J/(Km^3)}$, $\alpha_c = 0.002\,\mathrm{kg/\ (m^3\,s)}$, $w_k = 0.004\,\mathrm{m}$). This example has been chosen because misclassifications of soil type usually occur between neighbored classes. Choosing a soil type from the other edges of the soil texture triangle (e.g., silt, clay), however, provides greater differences than those evaluated here. Note that land-use is distributed as in the reference simulation.

The fluxes of sensible heat slightly increase for uniformly sandy loam as compared to the reference simulation. On the contrary, the latent heat fluxes, on average, decrease for the former as compared to the latter (see evapotranspiration in Fig. 7). Consequently, on average, the Bowen-ratios shift towards higher values for the uniformly sandy loam (not shown). This shift is opposite to the effect on the Bowen-ratio provided by a doubled field capacity, an emissivity equal to 1, a 10%-increased thermal diffussivity or volumetric heat capacity.

The uniform soil-type, of course, results in a more homogeneous distribution of soil heat fluxes, evapotranspiration (e.g., Fig. 7), soil wetness factors, and near-surface specific humidity than the heterogeneous soil distribution of the reference simulation. In the distributions of evapotranspiration and surface temperatures, areas of different land-use may be distinguished clearly. Thus, the knowledge of land-use distribution is also an important prerequisite to adequately simulate the surface fluxes and variables of state.

In the case of sandy loam, the lower ABL is slightly warmer and drier than in the reference simulation. At some locations, air temperatures or humidity of the reference and this simulation differ more than 0.5 K and 0.5 g/kg, respectively.

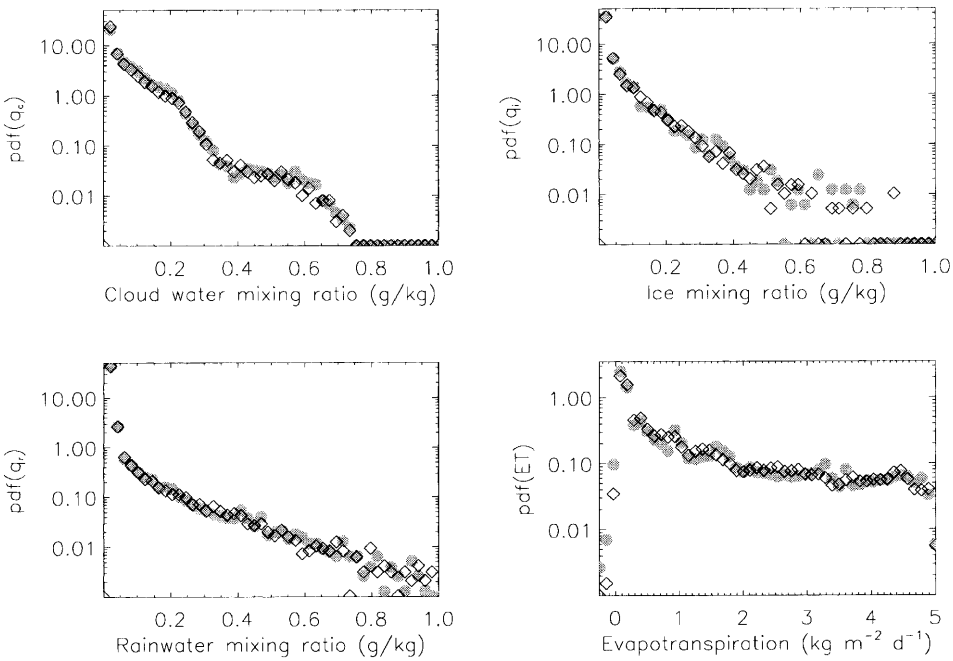

Fig. 7. Like Fig. 2, but for the reference simulation (gray circles) and the simulations with sandy loam throughout the domain

Cloud fields form at the same places in the simulation with an uniformly sandy loam than in the reference simulation (therefore not shown), but their rainwater- and ice- mixing ratios are lower at the very beginning of the integration time due to the lower evapotranspiration (see also Fig. 7). Later on, however, the cloud fields are less horizontally extended. The different heating and water vapor supply to the atmosphere modify the cloud- and precipitation microphysical and related dynamical processes (see also Fig. 7). Thus, differences in cloud- and precipitating-particles grow with progressing simulation time. As compared with the reference simulation, the probability density functions are skewed towards lower values in the simulation with uniformly sandy loam (Fig. 7). Thus, the uniformly sandy loam results in a strongly altered precipitation pattern. Herein, the areas of maximum precipitation are shifted downstream. Note that this shift is in the opposite direction than that yielded by doubling roughness length.

4.4 Plant properties

There is a huge number of land surface schemes that use a similar "big-leaf/big-stoma"-approach and a Jarvis-type (Jarvis, 1976) bulk-stomatal resistance approach like that applied here (e.g., Groß, 1988; Schlünzen, 1994; Kramm et al., 1996; Chen and Dudhia, 2000; Mölders et al., 1999). Since previous studies addressed the impact of minimum stomatal resistance on evaporative fluxes (e.g., Collin and Avissar, 1994; Gao et al., 1996) here focus is on area weighted fluxes, cloud- and precipitating-particles.

4.4.1 Evaporative conductivity

Maximum and minimum stomatal conductivity corresponds to the reciprocal value of minimum and maximum resistance. In the immediate vicinity of a leaf, the micrometeorological conditions differ from those of other leafs within the same canopy. Moreover, the micrometeorological conditions continuously vary because of the changing positions of the leafs (e.g., inclination, orientation, height of stand, shading, ventilation, etc.). Obviously, stomata assimilate quickly to the continuously altering micrometeorological conditions. Therefore, stomatal resistances range over several orders of magnitude although the stand is seemingly homogeneous (e.g., Körner et al., 1979; Avissar, 1991; Bonan et al., 1993). Due to this variability latent heat fluxes may differ appreciably over even small distances in nature.

Data from more than 1000 measurements of relative stomatal resistance and their frequencies

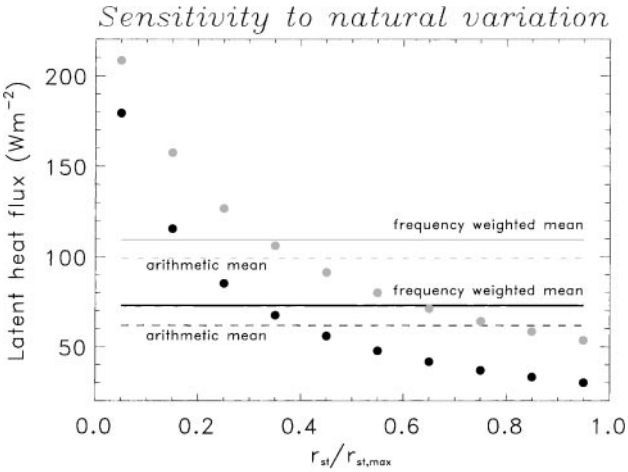

Fig. 8. Latent heat fluxes as a function of the relative stomatal resistance, $r_{st}/r_{st,\max}$ for maximum stomatal resistances of $r_{st,\max} = 500$ s/m (gray) and $r_{st,\max} = 1000$ s/m (black), respectively. The solid line denotes the latent heat flux weighted by the relative stomatal resistance. The dashed line stands for the latent heat flux simulated by use of the arithmetic average of $r_{st}/r_{st,\max}$ (see text for discussion)

that were performed over an area of 3 m radius under relative constant atmospheric conditions (Avissar, 1991) are used to examine the sensitivity of latent heat fluxes to stomatal resistance. In so doing, latent heat fluxes are determined for the relative stomatal resistances of 0.05 to 0.95 in steps of 0.1 assuming maximum stomatal resistances of 500 s/m and 1000 s/m, respectively. Figure 8 illustrates that the area-aggregated fluxes cannot be calculated by use of the arithmetic averages of the surface characteristics (here that of the stomatal resistance). Latent heat fluxes determined by use of the arithmetic mean of the stomatal resistance underestimate the area-mean latent heat flux (Fig. 8). The latter is (physical correctly) determined by calculating the fluxes for the various stomatal resistances and frequency-weighting the resulting fluxes. The resulting latent heat fluxes differ by about 12% and 18% for a maximum stomatal resistance of 1000 s/m and 500 s/m, respectively (Fig. 8).

To examine the uncertainty due to evaporative conductivity, the values of this parameter are doubled. The impact of stomatal conductance on the surface fluxes found by other authors (e.g., Collins and Avissar, 1994; Gao et al., 1996) is also manifested by the results of the present study, but it seems to be less great under the synoptic conditions assumed here. These discrepancies can be explained by the fact that these authors performed off-line simulations. In the present study, three-dimensional simulations in coastal mid-latitude areas in spring are performed. Here, compared with the reference simulation the fluxes of latent heat decrease slightly.

The ABL and the soil will heat slightly more if maximum evaporative conductivity is doubled. Furthermore, the amount of cloud- and precipitation particles as well as the horizontal extension of the precipitation fields decrease slightly (not shown). Therefore, slightly less precipitation occurs. In areas of high Bowen-ratios in the reference simulation, the Bowen-ratios grow for a doubling of evaporative conductivity. This seemingly small sensitivity results from the fact that under the meteorological situation of this study, maximum conductivity is seldom achieved.

4.5 Subgrid-scale heterogeneity and inhomogeneity

In the last decade, there were large efforts to consider subgrid-scale surface heterogeneity in mesoscale modeling (see Giorgi and Avissar, 1997). Several authors parameterized subgrid-scale heterogeneity by statistical-dynamical approaches (e.g., Wetzel and Chang, 1988; Entekhabi and Eagleson, 1989; Avissar, 1991; 1992) as also demonstrated in subsection 4.4.1. Mixture strategies, wherein tightly coupled energy balances (describing the heterogeneity at the micro-scale) are determined for the different surface types, are used in several GCM surface modules (e.g., Sellers et al., 1986; Dickinson et al., 1986) and chemical boundary layer models (Kramm et al., 1994). On contrary, the mosaic approach (e.g., Avissar and Pielke, 1989) neglects all small scale interactions by assuming that the various homogeneous surface patches within a grid-cell interact independently of each other with a well-mixed atmosphere. Area-weighted averages of surface fluxes are determined for the exchange with the atmospheric surface layer. Varieties of the mosaic approach are the blending height concept (e.g., Claussen, 1991) or the so-called mountain approach (e.g., Leung and Ghan, 1995). The results obtained by the mixture and mosaic approach showed only small effective differences over a wide range of conditions (Koster and Suarez, 1992). A limitation of both the mixture and

mosaic approach is the use of a mean atmospheric forcing and that the locations where the fluxes occur are more or less unknown. The explicit subgrid-scheme (e.g., Seth et al., 1994; Mölders et al., 1996) allows that unique energy and hydrological budgets are maintained for each subgrid cell using the forcing at the respective location within the subgrid cell, i.e. the location of the fluxes is known. If the mosaic approach or the explicit subgrid-scheme are alternatively applied for episodes with precipitation, the results will differ strongly with respect to the partitioning of net radiation between the fluxes of sensible and latent heat as well as cloud- and precipitation-formation (Mölders et al., 1996). Then the mosaic approach yields higher Bowen-ratios than the explicit subgrid-scheme (Mölders et al., 1996). However, when using the same parameterization of the near-surface forcing these schemes provide the same results as long as no heterogenization of precipitation is considered or no precipitation occurs.

In the present study, a special effect, namely that of inhomogeneity will be addressed and compared to simple heterogeneity and to the strategy of dominant land-use (reference simulation). The latter means that the dominant land-use type within a grid-cell is assumed to be the representative one for the determination of surface fluxes. In contrast to the strategy of dominant land-use and most of the other schemes mentioned above, the explicit subgrid-scheme allows to heterogenize the fluxes (subgrid-scale heterogeneity) and precipitation within a grid-cell (subgrid-scale heterogeneity plus inhomogeneity). Thus, it is able to consider subgrid-scale inhomogeneity effects.

4.5.1 Strategy of dominant land-use vs. subgrid-scale heterogeneity

When subgrid-scale heterogeneity is considered, the fraction of strongly evapotranspiring land-use types is lower than in the reference simulation (see Fig. 1). Therefore, on average, the latent heat fluxes decrease (Fig. 9) and the ABL is drier (up to 0.5 g/kg) in the former than the latter. The greatest differences in specific humidity occur where the characteristics of the dominating land-use type differ very strongly from those of the non-dominating land-use types within a grid-cell (e.g., over the boundaries of suburbs or along the coast). Herein, the degree of heterogeneity seems to be of less importance.

4.5.2 Strategy of dominant land-use vs. subgrid-scale heterogeneity plus subgrid-scale inhomogeneity

In the case that subgrid-scale heterogeneity or subgrid-scale heterogeneity plus inhomogeneity are considered, cloud-base height seems to be closely related to the heterogeneity of the underlying surface. The reason is the more continuous water supply to the atmosphere by large, homogeneous than heterogeneous areas. For the latter, grid-cell area-averaged evapotranspiration may be appreciably influenced by subgrid-scale land-use and (if existent) inhomogeneity (see also Fig. 9).

In the ABL in areas of high degree of heterogeneity, air temperatures will achieve significantly higher (more than 0.5 K in the daily average in the first layer above ground) values than in the reference simulation if subgrid-scale heterogeneity and inhomogeneity are taken into account.

Under consideration of heterogeneity plus inhomogeneity vertical motions are enhanced and the clouds reach higher than in the reference case. Moreover, a more shower-like precipitation occurs, because the precipitation formation via the ice phase is increased in the former as compared to the latter (e.g., Fig. 9).

4.5.3 Subgrid-scale heterogeneity vs. subgrid-scale heterogeneity plus subgrid-scale inhomogeneity

If subgrid-scale inhomogeneity is taken into account, after a precipitation event, inhomogeneity arises. It leads to different soil moisture, soil- and ground temperatures, and thus, to different soil heat fluxes, sensible and latent heat fluxes in areas of same land-use within a grid-cell (e.g., Figs. 9a,b, 10). Consequently, the Bowen-ratios shift towards lower values as compared to the case where only subgrid-scale heterogeneity is considered. However, they are, on average, higher than in the reference simulation (e.g., Fig. 10).

On average, at day, soils will heat more strongly if subgrid-scale inhomogeneity is additionally considered. In this latter case, the grid-cell area-averaged surface temperatures show up to

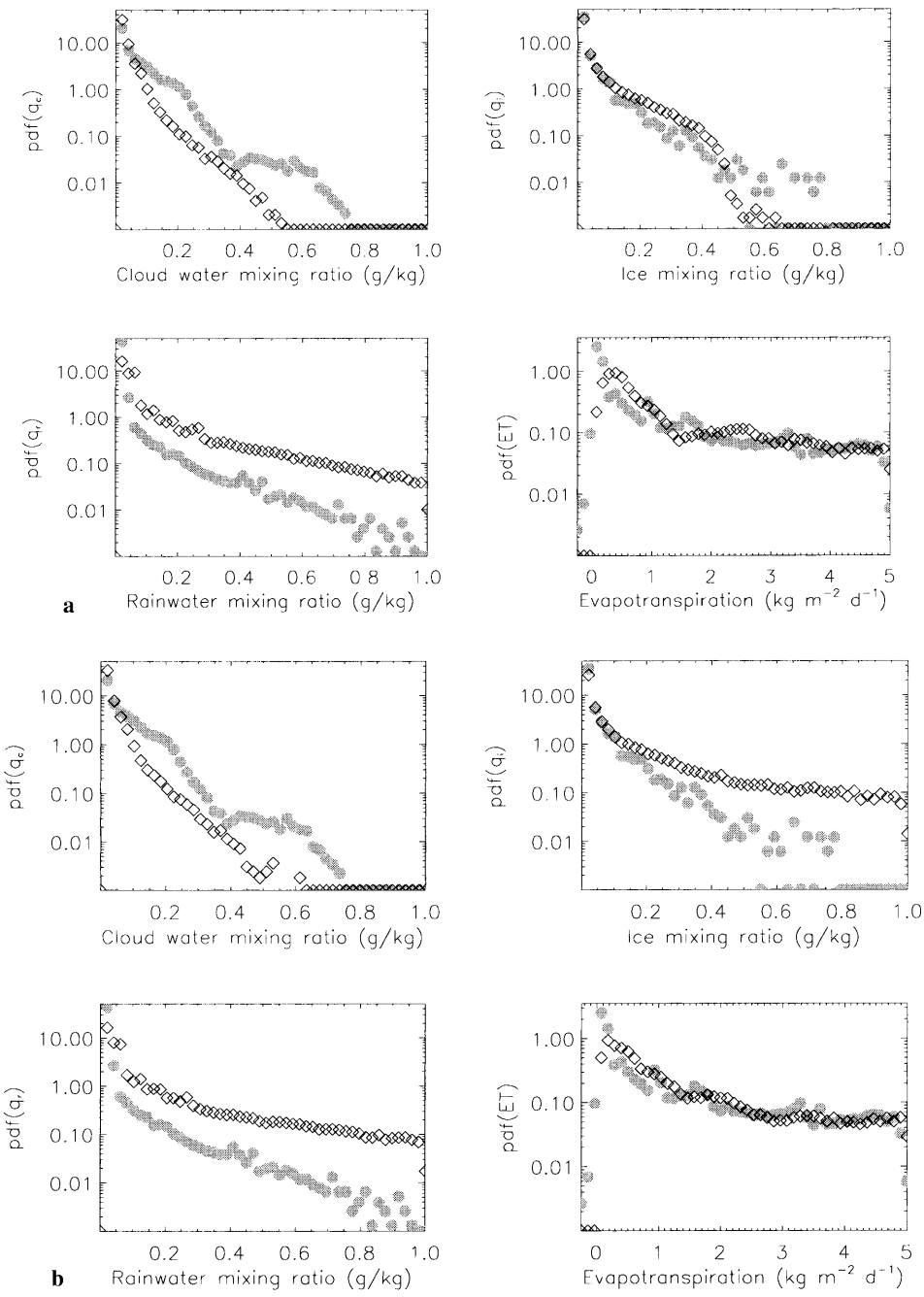

Fig. 9. Like Fig. 2, but **a** for the reference simulation (gray circles) and the simulation with subgrid-scale heterogeneity (diamonds), as well as **b** for the reference simulation (gray circles) and the simulation with subgrid-scale heterogeneity and inhomogeneity (diamonds)

2 K higher values that result among other from the reduced cloudiness (see also Fig. 9). There exists a shift towards higher frequencies of lower ice- and rainwater mixing ratios as compared to the simulation without subgrid-scale inhomogeneity, but with heterogeneity.

4.6 Similarity

The similarity coefficients between the reference and the altered plant- and soil-parameter distribution amount 0.9999, 0.9999, 0.9846, 0.9898, 0.9926, 0.9941, 0.9951, and 0.9956 for thermal

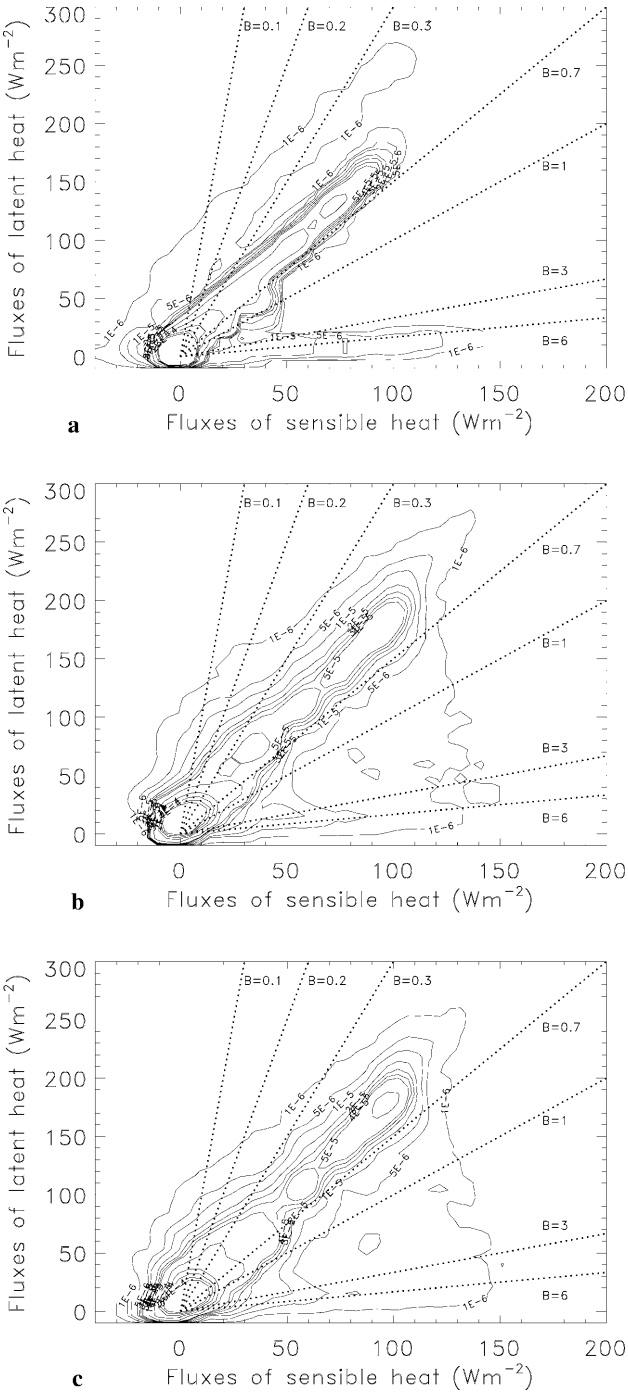

Fig. 10. Isolines of joint probability density functions for the surface fluxes of latent and sensible heat in **a** the reference simulation, **b** the simulation with subgrid-scale heterogeneity, as well as **c** the simulation with subgrid-scale heterogeneity and inhomogeneity. Lines of constant Bowen ratios are superimposed

diffusivity, volumetric heat capacity, emissivity, albedo, roughness length, field capacity, capillarity, and maximum evaporative conductivity, respectively. In the case of the simulation with inclusion of subgrid-scale heterogeneity, the similarity coefficients amount 0.8303, 0.8052, 0.8344, 0.8521, 0.8677, 0.8857, 0.8975, and 0.8869 for thermal diffusivity, volumetric heat capacity, emissivity, albedo, roughness length, field capacity, capillarity, and maximum evaporative conductivity, respectively. This means that, as compared to the reference data, some of the alterations performed yield to a more dissimilar initial distribution of the respective plant- or soil-parameters than others, although all parameters are varied within the range of their natural variability.

The simulated fields of the wind vector components, specific humidity and air temperature (all taken at reference height) as well as the fluxes are similar before sunrise (Fig. 11). Moreover, these quantities and fluxes are less influenced by the uncertainty of soil- and plant-parameters in the early afternoon than before noon or later in the afternoon or early evening (Fig. 11). However, there exists a greater uncertainty for field capacity, capillarity, emissivity, volumetric heat capacity, thermal diffusivity, and soil type than for albedo (Fig. 11). The greatest dissimilarities in specific humidity, air temperatures and the *u*-component of the wind-vector occur for field capacity, emissivity, and thermal diffusivity about two hours after sunrise (Fig. 11). The simulated distributions are less similar for specific humidity than for air temperature as well as the *v*- and *w*-components of the wind-vector (e.g., Fig. 11).

The similarity coefficients show that the partitioning of the excess water vapor between cloud water and ice can be appreciably affected by the choice of field capacity, capillarity, volumetric heat capacity, thermal diffusivity, and surface emissivity (Fig. 11). Note that these findings are also manifested by the probability density functions and student-t-tests. The fields of the cloud- and precipitating-particles are less similar in the lower than in the upper troposphere (not shown). Here, the largest dissimilarities occur for cloud water and ice (see also Fig. 11). This dissimilarity means that the cold- and warm-path microphysical processes are significantly altered for field capacity, capillarity, volumetric heat capacity, and thermal diffusivity. Consequently, onset and intensity of precipitation are changed, too (see also Fig. 11).

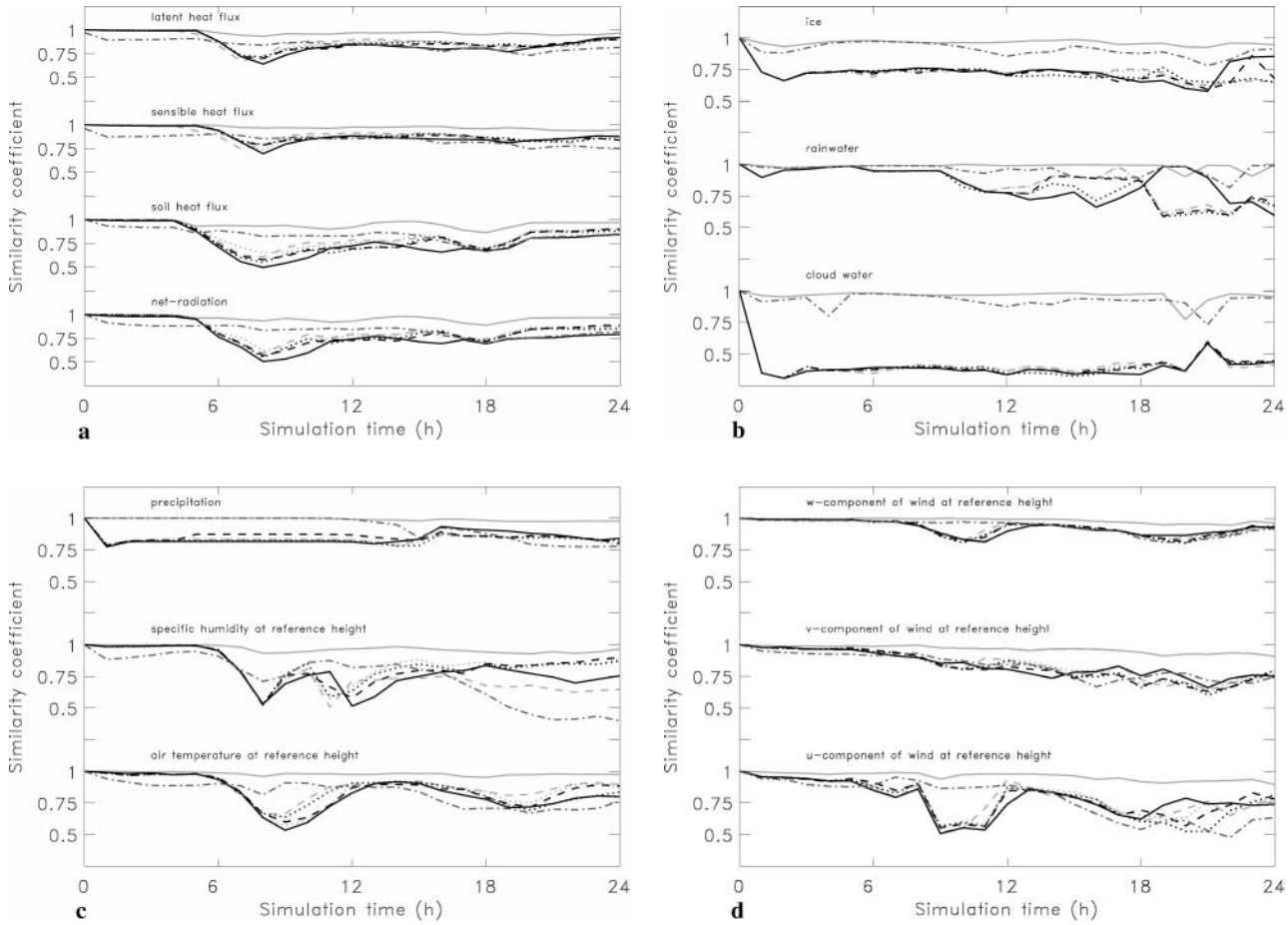

Fig. 11. Temporal development of similarity coefficients as obtained for **a** the energy- and water fluxes, **b** cloud- and precipitating-particles, **c** precipitation, specific humidity and air temperature both at reference height, as well as **d** the components of the wind vector for altered albedo (grey solid lines), field capacity (gray dotted lines), capillarity (gray dashed lines), emissivity (black solid lines), volumetric heat capacity (black dotted lines), thermal diffusivity (black dashed lines), subgrid-scale heterogeneity plus inhomogeneity (black dash-dotted lines), respectively

The uncertainty caused by field capacity, capillarity, volumetric heat capacity, and thermal diffusivity exceeds that resulting from subgrid-scale heterogeneity and inhomogeneity (e.g., Fig. 11). Nevertheless, as mentioned above, the parameter fields are more similar for the former than the latter.

6. Conclusions

The sensitivity of mesoscale simulation results to the choice of soil- and plant-parameters is explored using GESIMA's land surface scheme. Similar land surface schemes exist in METRAS (Schlünzen, 1994) or FITNAH (Groß, 1988), for instance. In addition, there are many land surface schemes that apply some of the parameterizations used in this study like (1) a two-layer force-restore-method to determine soil wetness (e.g., Deardorff, 1978; Jacobson and Heise, 1982), (2) a Jarvis-type approach (Jarvis, 1976) to calculate transpiration (e.g., Kramm et al., 1994; 1996; Dudhia and Chen, 2000; Mölders et al., 1999), or (3) the heat diffusion equation under the assumption that soil moisture and heat fluxes can be treated as being decoupled (e.g., McCumber and Pielke, 1981; Dudhia and Chen, 2000).

The design of the study was to define a reference case, vary each parameter or condition one at a time for all land-use- and soil-types within the entire model domain and examine the model responses. The results substantiate that, in addition to the simulated water- and energy-fluxes, the choice of the soil- and plant-parameters

may also appreciably affect the variables of state as well as cloud- and precipitation-formation. Herein, however, the various plant- and soil-parameters affect differently the simulated quantities at different times of the day, i.e. the uncertainty depends on time (Fig. 11). Except for the cloud- and precipitating-particles, the simulated results are less influenced by the uncertainty of the soil- and plant-parameter at night and in the early afternoon than at the other time of the day. This surprising time-dependency of uncertainty suggests that evaluation of meteorological models should be performed at those times of the day when the uncertainty in model results caused by the choice of plant- and soil-parameters is at a minimum. Thus, obtaining seemingly right predictions which by chance may be caused by the choice of the plant- and/or soil-parameters can be avoided. Further, one may conclude that domain-specific parameters, i.e. parameters determined for the region and time under study, should be used when available. This also means that parameter sets should be updated when the model domain is changed, instead of using an universal parameter set for all applications.

At some locations, the simulated values may differ appreciably or even significantly for all sensitivity studies. The partitioning of net radiation shifts towards higher Bowen-ratios for an increased roughness length or a sandy loam, heterogeneity and inhomogeneity, while it is skewed towards lower values for an emmissivity equal to 1, increased thermal diffussivity, volumetric heat capacity or capillarity. On average, consideration of inhomogeneity decreases slightly the Bowen-ratios, but they are still higher than in the reference simulation that applied the strategy of dominant land-use.

The distribution of the precipitation fields is shifted upstream by about 4 km when roughness length is doubled, while it shifts downstream by about 4 km when a uniformly sandy loam is assumed in the entire model domain. Albedo affects to a high degree the extension of the precipitation fields as well as the intensity of precipitation. Surface emissivity, roughness length, thermal diffusivity, volumetric heat capacity, field capacity, capillarity, heterogeneity and inhomgeneity appreciably influence the statistical behavior of the surface fluxes, variables of state as well as cloud- and precipitating-particles. Note that, here, the impact of roughness length as well as evaporative conductivity is less strong than that found in offline studies by other authors (e.g., Collins and Avissar, 1994; Gao et al., 1996).

Considering all these findings, one may conclude that it is an urgent need to develop parameterizations that consider the variability range of the aforementioned parameters. These parameterizations, however, require to put up data sets of the frequency distributions of these parameters.

In the force-restore-approach, the simulated results are only slightly sensitive to the choice of field capacity under the synoptic situation examined here. Since albedo, roughness length, emmissivity, soil type and soil hydraulic characteristics may appreciably affect precipitation and its distribution it is an urgent need to derive appropriate parameter sets for these quantities, especially, for studies on water availability.

The results also show that the results obtained by the reference simulation and the simulation with subgrid-scale heterogeneity including inhomogeneity are more similar than those of the reference simulation and the simulations with altered soil- and plant-parameters. This greater similarity suggests that the choice of the plant- and soil- parameters can more strongly influence the simulated results than subgrid-scale heterogeneity including inhomogeneity. However, the uncertainty caused by subgrid-scale heterogeneity including inhomogeneity demands that these effects should be considered by soil-vegetation-atmosphere-schemes, especially when they are applied for studies on water availability.

Acknowledgments

I would like to express my thanks to G. Kramm, K.E. Erdmann, A. Ziemann, and the anonymous reviewers for fruitful discussion and helpful comments. Thanks also to K. Friedrich for providing the land-use data. This study was financially supported by the DFG under contracts Mo770/1-1, Mo770/1-2 and Mo770/2-1 as well as by the BMBF under contract 01LA98494, for which I wish to thank.

References

Anderson DA, Tannehill RH, Fletcher A (1984) Computational fluid dynamics and heat transfer. Hemispheric Publishing Corporation, New York

Avissar R, Pielke RA (1989) A parameterization of heterogeneous land surface for atmospheric numerical models

and its impact on regional meteorology. Mon Wea Rev 117: 2113–2136

Avissar R (1991) A statistical-dynamical approach to parameterize subgrid-scale land-surface heterogeneity in climate models. Surv Geophys 12: 155–178

Avissar R (1992) Conceptual aspects of a statistical-dynamical approach to represent landscape subgrid-scale heterogeneity in atmospheric models. J Geophys Res 97(D3): 2729–2742

Baumgartner A, Mayer H, Metz W (1977) Globale Verteilung der Oberflächenalbedo. Meteor Rundsch 29: 28–43

Baumgartner A, Liebscher H-J (1990) Lehrbuch der Hydrologie, Bd. 1: Allgemeine Hydrologie – Quantitative Hydrologie. Gebrüder Bornträger, Berlin, Stuttgart, 673 pp

Bear J (1988) Dynamics of fluids in porous media. Dover, New York, 764 pp

Betts AK, Ball JH (1997) Albedo over the boreal forest. J Geophys Res 102D: 28901–28909

Blackadar AK (1962) The vertical distribution of wind and turbulent exchange in a neutral atmosphere. J Geophys Res 67: 3095–3103

Bonan GB, Pollard D, Thompson SL (1993) Influence of subgrid-scale heterogeneity in leaf area index, stomatal resistance, and soil moisture on grid-scale land-atmosphere interactions. J Climate 6: 1882–1897

Businger JA, Wyngaard JC, Izumi Y, Bradley EF (1971) Flux profile relationship in the atmospheric surface layer. J Atmos Sci 28: 181–189

Charney J (1975) Dynamics of desert and droughts in the Sahel. Quart J Roy Meteor Soc 101: 193–202

Chen F, Dudhia J (2000) Coupling an advanced land surface hydrology model with the Penn State/NCAR MM5 modeling system, Part 1: Model description and implementation. Mon Wea Rev (in press)

Claussen M (1988) On the surface energy budget of coastal zones with tidal flats. Contrib Atmos Phys 61: 39–49

Claussen M (1991) Estimation of areally-averaged surface fluxes. Boundary Layer Meteor 54: 387–410

Collins DC, Avissar R (1994) An evaluation with the Fourier amplitude sensitivity test (FAST) of which land-surface parameters are of greatest importance in atmospheric modeling. J Climate 7: 681–703

Cuenca R, Ek M, Mahrt L (1996) Impact of soil water property parameterization on atmospheric boundary layer simulation. J Geophys Res 101D: 7269–7277

Deardorff JW (1978) Efficient prediction of ground surface temperature and moisture, with inclusion of a layer of vegetation. J Geophys Res 84C: 1889–1903

De Fries RS, Field CB, Fung I, Justice CO, Los S, Matson PA, Matthews E, Mooney HA, Potter CS, Prentice K, Sellers PJ, Townshend JRG, Tucker CJ, Ustin SL, Vitousek PM (1995) Mapping the land surface for global atmosphere-biosphere models: toward continuous distributions of vegetation's functional properties. J Geophys Res 100D: 20867–20882

Devantier R, Raabe A (1996) Application of a quasispectral cloud parameterization scheme to a mesoscale snowfall event over the Baltic Sea. Contrib Atmos Phys 69: 375–384

Dickinson RE, Henderson-Sellers A, Kennedy PJ, Wilson MF (1986) Biosphere-atmosphere transfer scheme (BATS) for the NCAR community climate model, NCAR Technical Note 275+STR

Dorman JL, Sellers PJ (1989) A global climatology of albedo, roughness length and stomatal resistance for atmospheric general circulation models as represented by the simple biosphere model (SiB). J Appl Meteor 28: 833–855

Eagleson PS (1982) Ecological optimality in water-limited soil-vegetation systems: 1. Theory and hypothesis. Water Resour Res 18: 323–340

Entekhabi D, Eagleson P (1989) Land surface hydrology parameterization for atmospheric general circulation models including subgrid-scale spatial variability. J Climate 2: 816–831

Entekhabi D, Brubaker KL (1995) An analytical approach to modeling land-atmosphere interaction, 2. Stochastic formulation. Water Resour Res 31: 633–643

Eppel DP, Kapitza H, Claussen M, Jacob D, Koch W, Levkov L, Mengelkamp H-T, Werrmann N (1995) The nonhydrostatic mesoscale model GESIMA, Part II: Parameterizations and applications. Contrib Atmos Phys 68: 15–41

Friedrich K (1999) Numerische Untersuchungen zur Sensitivität des Bowen-Verhältnisses. Master Thesis, Inst Meteor, Univ Leipzig (available from the author)

Friedrich K, Mölders N, Tetzlaff G (2000) On the influence of surface heterogeneity on the Bowen-ratio: A theoretical case study. Theor Appl Clim 65: 181–196

Fritsch H (1999) Parametrisierung von Bodenfeuchte und Bodentemperatur für ein mesoskaliges Modell. Master Thesis Inst Meteor Univ Leipzig (available from the author)

Garratt JR (1992) The internal boundary layer – a review. Boundary Layer Meteorol 50: 171–203

Gao X, Sorooshian S, Gupta HV (1996) Sensitivity studies of the biosphere-atmosphere transfer scheme. J Geophys Res 101D: 7279–7289

Giorgi F, Avissar R (1997) Representation of heterogeneity effects in earth system modeling: Experience from land surface modeling. Rev Geophys 35: 413–438

Groß G (1988) A numerical estimation of the deforestation effects on local climate in the area of the Frankfurt International Airport. Contrib Atmos Phys 61: 219–231

Hantel M, Acs F (1998) Physical aspects of the weather generator. J Hydrol 212–213: 393–411

Hicks BB, Baldocchi DD, Meyers T-P, Hosker RP Jr, Matt RP (1987) A pre-liminary multiple resistance routine for deriving dry deposition velocities from measured quantities. Water, Air, and Soil Pollution 36: 311–330

Hinneburg D, Tetzlaff G (1996) Calculated wind climatology of the South-Saxonian/North-Czech mountain topography including an improved resolution of mountains. Ann Geophys 14: 767–772

Hupfer P, Raabe A (1994) Meteorological transition between land and sea in the microscale. Meteorol Zeitsch 44: 100–103

Idso SB, Jackson RD, Reginato RJ, Kimball BA, Nakayama FS (1975) The dependence of bare soil albedo on soil water content. J Appl Meteor 14: 109–113

Jackson DA, Somers KM, Harvey HH (1989) Similarity coefficients: Measures of co-occurrence and association or simply measures of occurrence? Am Natur 133: 436–453

Jacobson I, Heise E (1982) A new economic method for the computation of the surface temperature in numerical models. Contrib Atmos Phys 55: 128–141

Jarvis PG (1976) The interpretation of the variations in leaf water potential and stomatal conductance found in canopies in the field. Phil Trans R Soc London B273: 593–610

Kapitza H, Eppel DP (1992) The non-hydrostatic mesoscale model GESIMA, Part I: Dynamical equations and tests. Contrib Phys Atmos 65: 129–146

Körner C, Scheel JA, Bauer H (1979) Maximum leaf diffusive conductance in vascular plants. Photosynhetica 13: 45–82

Koster RD, Suarez MJ (1992) A comparative analysis of two land surface heterogeneity representations. J Climate 5: 1379–1390

Kramm G, Dlugi R, Mölders N, Müller H (1994) Numerical investigations of the dry deposition of reactive trace gases. In: Baldasano JM, Brebbia CA, Power H, Zannetti P (eds.) Air Pollution II Vol. 1: Computer Simulation. Computational Mechanics Publications, Southampton, Boston, 285–307

Kramm G (1995) Zum Austausch von Ozon und reaktiven Stickstoffverbindungen zwischen Atmosphäre und Biosphäre. Maraun-Verlag, Frankfurt, 268 pp

Kramm G, Dlugi R, Dollard GJ, Foken T, Mölders N, Müller H, Seiler W, Sievering H (1995) On the dry deposition of ozone and reactive nitrogen compounds. Atmos Environ 29: 3209–3231

Kramm G, Beier N, Foken T, Müller H, Schröder P, Seiler W (1996) A SVAT scheme for NO, NO_2, and O_3 – model description. Meteorol Atmos Phys 61: 89–106

Leung LR, Ghan SJ (1995) A subgrid parameterization of orographic precipitation. Theoret Appl Met 47: 95–118

Levkov L, Rockel B, Kapitza H, Raschke E (1992) 3D mesoscale numerical studies of cirrus and stratus clouds by their time and space evolution. Contrib Atmos Phys 65: 35–58

McCumber M, Pielke RA (1981) Simulation of the effects of surface fluxes of heat and moisture in a mesoscale numerical model soil layer. J Geophys Res 86: 9929–9938

Mellor GL, Yamada T (1974) A hierarchy of turbulence closure models for planetary boundary layers. J Atmos Sci 31: 1791–1806

Mölders N, Raabe A (1996) Numerical investigations on the influence of subgrid-scale surface heterogeneity on evapotranspiration and cloud processes. J Appl Meteor 35: 782–795

Mölders N, Raabe A, Tetzlaff G (1996) A comparison of two strategies on land surface heterogeneity used in a mesoscale β meteorological model. Tellus 48A: 733–749

Mölders N, Strasser U, Schneider K, Mauser W, Raabe A (1997a) A sensitivity study on the initialization of surface characteristics in meso-β/γ-modeling using digitized vs. satellite derived land-use data. Contrib Atmos Phys 70: 173–187

Mölders N, Kramm G, Laube M, Raabe A (1997b) On the influence of bulk-parameterization schemes of cloud microphysics on the predicted water-cycle relevant quantities – a case study. Meteorol Zeitschr 6: 21–32

Mölders N (1998) Landscape changes over a region in East Germany and their impact upon the processes of its atmospheric water-cycle. Meteor Atmos Phys 68: 79–98

Mölders N (1999) On the effects of different flooding stages of the Odra and different landuse types on the local distributions of evapotranspiration, cloudiness and rainfall in the Brandenburg-Polish border area. Contrib Atmos Phys 72: 1–24

Mölders N, Haferkorn U, Knappe S, Döring J, Kramm G (1999) Evaluation of simulated water budget by means of measurements at Brandis lysimeter station. In: Tetzlaff G, Grünewald U (eds.) 2. Tagung des Fachausschusses Hydrometeorologie am 15./16. November 1999 in Leipzig. Mitt Leipzig 16: 67–83

Ogunjemiyo S, Schuepp PH, MacPherson I, Dejardins RL (1997) Analysis of flux maps versus surface characteristics from Twin Otter grid flights in BOREAS 1994. J Geophys Res 102: 29135–29145

Oke TR (1978) Boundary layer climates. Routledge, London/New York, 435 pp

Olberg M, Rakóczi F (1984) Informationstheorie in der Meteorologie und Geophysik. Akademie Verlag, Berlin, 181 pp

Orlanski I (1976) A simple boundary condition for unbounded hyperbolic flows. J Comp Phys 21: 251–269

Pielke RA (1984) Mesoscale Meteorological Modelling. Academic Press, Inc, London, 612 pp

Pielke RA, Rodriguez JH, Eastman JL, Walko RL, Stocker RA (1993) Influence of albedo variability in complex terrain on mesoscale systems. J Climate 6: 1798–1806

Raabe A (1983) On the relation between the drag coefficient and fetch above the sea in the case of off shore wind in the near-shore zone. Z Meteor 6: 363–367

Schlünzen HK (1994) Mesoscale modeling in complex terrain: an overview on the German nonhydrostatic models. Contrib Atmos Phys 67: 243–253

Sellers PJ, Mintz Y, Sud YC, Dalcher A (1986) A simple biosphere atmosphere model (SiB) for use within general circulation models. J Atmos Sci 43: 505–531

Seth A, Giorgi F, Dickinson RE (1994) Simulating fluxes from heterogeneous land surfaces: explicit subgrid method employing the biosphere-atmosphere transfer scheme (BATS). J Geophys Res 99D: 18651–18667

Shao Y, Iranneiad P (1999) On the choice of soil hydraulic models in land-surface schemes. Boundary Layer Meterol 90: 83–115

Smolarkiewicz PK (1984) A fully multidimensional positive definite advection transport algorithm with small implicit diffusion. J Comp Phys 54: 325–362

Wetzel PJ, Chang J-T (1988) Evapotranspiration from nonuniform surfaces: A first approach for short-term numerical weather prediction. Mon Wea Rev 116: 600–621

Wilson MF, Henderson-Sellers A, Dickinson RE, Kennedy PJ (1987) Sensitivity of the biosphere-atmosphere transfer scheme (BATS) to the inclusion of variable soil characteristics. J Climate Appl Meteor 26: 341–362

Wünsche M (1995) Kippenböden, Rekultivierung und Gestaltung der Bergbaufolgelandschaft im Braunkohlerevier Westsachsens. In: Zukunft Südraum Leipzig. Beitr zu Lehre u Forschung der HTWK, 21–30

Zeng X, Pielke RA (1995) Further study on the predictability of landscape-induced atmospheric flow. J Atmos Sci 52: 1680–1698

Author's address: N. Mölders, Geophysical Institute, University of Alaska Fairbanks, P.O. Box 757320, 903 Koyukuk Dr., Fairbanks, AK 99775-7320, USA (E-mail: carmennicolemold@aol.com)